Design, Modeling, and Control of a Novel Hybrid-Excited Flux-Bidirectional-Modulated Generator-Based Wind Power Generation System

Qingsong Wang and Shuangxia Niu, *Member, IEEE*

***Abstract*—This paper proposes a novel hybrid excited generator, which is suitable for a variable-speed wind power generation system. Two sets of excitation sources are employed, which are permanent magnets (PMs) on the rotor and the field windings on the stator. The rotor is design with PM-iron structure, namely the PMs and iron poles are alternatively located in rotor, which can provide PM excitation and flux modulating simultaneously. Meanwhile, the adjacent stator teeth are designed with different height, which enables the stator with flux modulating effect, and, therefore, bidirectional flux modulating can be achieved. Some specific harmonics excited by the rotor PMs can be effectively adjusted by the field current, and the back electromotive force and electromagnetic torque can be regulated accordingly. Therefore, the proposed generator can achieve constant voltage control and maximum power point tracking control by controlling the field current. The design considerations and field regulating principle are analytically investigated. An improved Tabu search algorithm is used to optimize the proposed generator, and finite-element method is used to realize preliminary study of the electromagnetic performances. A prototype is manufactured and experimental tests are conducted to verify the theoretical analysis and control strategies.**

***Index Terms*—Bidirectional flux modulating, constant voltage, maximum power point tracking (MPPT) control, permanent magnet (PM)-iron structure.**

I. Introduction

SINCE fossil energy is nonrenewable and will cause environmental pollution, the development of clean energy systems is on an accelerating pace. Wind power as an environmentally clean and cost-effective energy source has attracted much attention in recent decades [1]–[4]. According to the statistic data provided by the Global Wind Energy Council, the global annual installed wind capacity has increased from 3.76G W at 2000 to 63.467 GW at 2015, and the growth trend will continue in the future [5].

Manuscript received February 20, 2017; revised April 9, 2017; accepted May 4, 2017. Date of publication May 15, 2017; date of current version January 3, 2018. This work was supported by the Research Grant Council, Hong Kong Special Administrative Region, China, under Projects PolyU 152130/14E and PolyU 15250916/16E. Recommended for publication by Associate Editor N. R Zargari. *(Corresponding author: Shuangxia Niu.)*

The authors are with the Department of Electrical Engineering, Hong Kong Polytechnic University, Kowloon, Hong Kong (e-mail: q.s.wang@connect.polyu.hk; eesxniu@polyu.edu.hk).

Color versions of one or more of the figures in this paper are available online at http://ieeexplore.ieee.org.

Digital Object Identifier 10.1109/TPEL.2017.2704103

Motivated by the increasing contribution of wind power generation systems (WPGS), the wind generator (WG) as a key component of WPGS is developed rapidly [6]–[10]. The squirrel-cage induction generator (SCIG) is a popular machine in WPGS due to its robust construction, low cost, and mechanical simplicity. No brushes are needed for the operation of SCIG, and a little maintenance is required [11]. The SCIG is mainly suitable for constant-speed WPGS, when the SCIG is used in variable-speed WPGS, a full-scale back-to-back converter is needed to connect the SCIG and the grid, which will increase the cost and reduce the efficiency. Another widely used WG is the doubly-fed induction generator (DFIG), which is suitable for variable-speed WPGS [12]–[14]. The stator of the DFIG is directly connected to the grid, while the rotor is connected to the grid through a back-to-back converter. The DFIG can perform well in a wide speed range from supersynchronous to subsynchronous speeds. Brushes or slip rings are needed in the DFIG, which is one of the main drawbacks of DFIG, and may result in electrical losses and machine failures. Both the SCIG-based WPGS and the DFIG-based WPGS cannot achieve direct drive, because it is difficult to design the SCIG and DFIG with multipole low-speed and high-torque capability. Gearboxes are usually used together with the SCIG and DFIG to reduce the speed and amplify the output torque, which inevitably reduce the efficiency and need routine maintenance. Therefore, direct-drive WPGS is more attractive due to the increased reliability.

Permanent-magnet synchronous generator (PMSG) is the most promising candidate in direct-drive WPGS due to its high torque density and high-efficiency features [15], [16]. The weight and size of the PMSG can be reduced when high-performance PMs are used. One disadvantage of the PMSG is its fixed PM excitation, so it is difficult to maintain constant output voltage when the wind speed varies. Hybrid-excited machines (HEMs) can well solve this problem; the magnetic field can be easily regulated by controlling the excitation current. Various HEMs have been proposed [17]–[20], and their application in WPGS are investigated in [21]–[23]. In order to achieve brushless structure, the existing HEMs usually employ both PM excitation and field coils on the stator [24]–[26]. The major drawbacks of the existing HEM configurations include: 1) Employing PMs on the stator will inevitably reduce the stator space for armature coils and the electromagnetic torque will be reduced; 2) the thermal condition of stator will be deteriorated

when employing all the excitation sources on the stator, and the PMs may suffer from demagnetization risk because the PMs are directly exposed to the stator thermal field.

The purpose of this paper is to propose a novel hybrid-excited flux-bidirectional-modulated generator (HE-FBMG), which is suitable for wide-speed range WPGS. In the proposed design, the PMs are employed on the rotor and field coils are employed on the stator, which can achieve better allocation of PM magnetic loading and electric loading, and, therefore, it can contribute to high torque density design. Meanwhile, the PMs avoid from being directly exposed to the stator heat, so the demagnetization risk of PMs is reduced. The configuration and design considerations are first discussed. The air-gap flux density, flux linkage, and back electromotive force (EMF) are studied analytically, which gives an insight into the working principle and field regulating theory of the proposed HE-FBMG. The control strategies including constant voltage control and maximum power point tracking (MPPT) control are studied. In order to achieve better overall performances, an improved Tabu search (ITS) algorithm [27] is used to optimal design the proposed generator, and its electromagnetic performances are investigated using finite-element method (FEM). Finally, the prototype is manufactured and its performances are studied through experimental tests. The proposed HE-FBMG-based WPGS is suitable for dc power supply, such as battery charging.

II. Configuration and Initial Design Considerations

A. Configuration of the HE-FBMG-Based WPGS

Fig. 1(a) shows the configuration of the HE-FBMG-based WPGS, and the proposed HE-FBMG is directly connected to the wind blade. The armature winding is connected to the load through a three-phase rectifying circuit, and the field winding is connected to a dc power supply. This system has simple structure and no mechanical gearbox is involved, which can improve the efficiency and reliability. With the merit of hybrid excitation, the back EMF and electromagnetic torque can be effectively controlled by the field current, which can simplify the control process. Meanwhile, thyristor-based-controlled rectifier in traditional WPGS can be replaced with diode-based uncontrolled rectifier in the proposed HE-FBMG-based WPGS, and the cost of hardware can be reduced consequently.

B. Structure of the HE-FBMG

Fig. 1(b) shows the structure of the proposed HE-FBMG, which consists of one rotor and one stator. PM-iron sequences, namely the PMs and iron poles are separated one by one, are employed on the rotor, which can provide PM excitation and flux modulation simultaneously. The field winding and armature winding are housed in the stator slots, both of which are concentrated windings. Compared with existing HEMs with both PMs and field coils on the stator, the proposed HE-FBMG can achieve better allocation of PM magnetic loading and electric loading. The spaces used for PMs and windings can be increased, which contributes to enhanced torque density. The demagnetization risk of PMs is also reduced, because the PMs

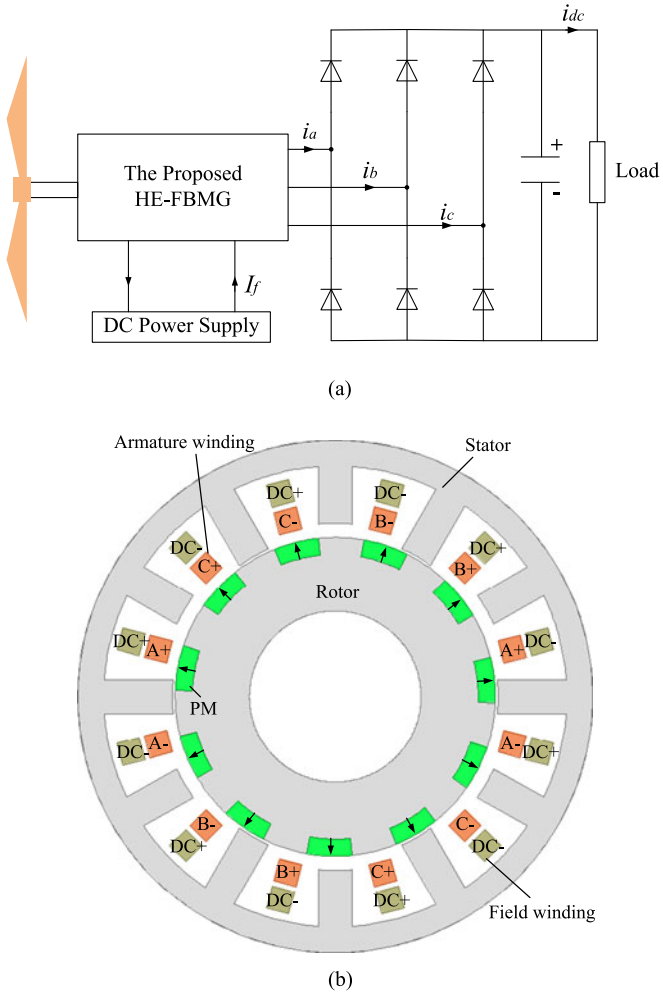

Fig. 1. Configuration of the HE-FBMG-based WPGS. (a) HE-FBMG-based WPGS. (b) Structure of the proposed HE-FBMG.

are not directly exposed in the stator thermal field. The adjacent stator teeth have the same width but different height, and, therefore, the stator teeth also have flux modulating effect, and the magnetic field excited by the PMs can be modulated to couple with the armature field.

The operating principle of the proposed HE-FBMG is based on the flux-modulating effect [28]–[31]. As can be seen from Fig. 1(b), both the armature winding and the field winding are concentrated wound on the stator teeth, and the pole-pair number (PPN) of the field winding p_f and the stator teeth number Ns satisfies

$$p_f = \frac{1}{2}Ns \tag{1}$$

and the PPN of the rotor PMs pr should be equal to the sum of the PPN of armature winding pa and PPN of the field winding p_f, as given in (2), which is similar to the pole-pair combination of magnetic gear [30]

$$pr = pa + pf = pa + \frac{1}{2}Ns. \tag{2}$$

Therefore, the proposed generator can be designed with large rotor PPN and operate at low-speed conditions. It should be

noted that direct-drive wind power generators in real applications usually have very large pole pairs and bulky size, in order to benefit the experimental verification, a scale-down prototype is studied instead in this paper.

C. Initial Design Considerations

In order to achieve an optimal matching between the aerodynamic of the turbine blade and the generator system, the generator should have variable speeds. According to the aerodynamic model of a wind turbine, the mechanical power that can be captured from the wind with a wind turbine is expressed as

$$Pm = \frac{1}{2}\rho_{\text{air}} Cp\left(\lambda, \theta\right) \pi r_b^2 v_\omega^3 \tag{3}$$

where ρair is the air mass density, Cp is the power coefficient, which is the function of the tip speed ratio λ (blade tip speed divided by wind speed) and the blade pitch angle θ, rb refers to the blade length, and $v\omega$ is the wind speed. The tip speed ratio λ is defined by

$$\lambda = \frac{\omega trb}{v\omega} \tag{4}$$

where ωt is the angular speed of the turbine shaft. Since the power coefficient is maximum for a constant tip speed ratio, the turbine shaft speed ωt should be controlled to be proportional to the wind speed $v\omega$, in order to capture maximum wind power.

In the proposed HE-FBMG-based WPGS, the mechanical power captured from the wind is directly transmitted to the wind turbine, which initially determines the size of the generator. The force density Fd (the force acting per unit surface area in the air gap) is given by

$$Fd \approx \frac{1}{2} \hat{Bg}\, \hat{As} \cos\left(\gamma\right) \tag{5}$$

where $\hat{Bg}$ is the amplitude of the fundamental component of the excitation flux density, $\hat{As}$ refers to the amplitude of the fundamental component of the stator surface current density in A/m, and γ is the angle between them. Since the flux density is limited by saturation, and the current density is limited by the heat dissipation, the force density is rather constant over a wide range of machine types and mainly influenced by the cooling condition.

With this force density, the power produced by a radial flux generator can be expressed as

$$P = \omega mT = \omega mrsF = 2\omega m\pi r_s^2 lsFd = 2\omega mVrFd \tag{6}$$

where ωm is the angular speed of the rotor, which is equal to ωt in direct drive WPGS, T is the torque, rs and ls are the air-gap radius and stack length, respectively, and Vr is the volume of the rotor. One can find that when cooling condition is determined, the force density is almost unchanged, and the generator power is mainly determined by the rotor speed and rotor volume.

The torque level of the generator can be derived from (3). In order to avoid excessive mechanical forces, wear, and audible noise, the blade tip speed must be limited. If the rated blade tip speed vt, rated is assumed independent of the generator size, then the angular speed of the rotor ωm is inversely proportional to the blade length rb. The rated torque can then be written as

$$T\text{rated} = \frac{P_{\text{rated}}}{\omega_{m,\text{rated}}} = \frac{rbP_{\text{rated}}}{v_{t,\text{rated}}} \propto r_b^3 \propto P_{\text{rated}}^{3/2}. \tag{7}$$

III. Mathematical Modeling of the HE-FBMG

The working principle of the proposed HE-FBMG is based on the flux bidirectional modulating effect. As can be seen from Fig. 1(b), the rotor is employed with PM-iron sequence, and the permeance difference between the PMs and the iron poles enables the flux modulating effect involved in the magnetic field excited by rotor PMs. Meanwhile, the stator also has flux modulating effect due to the uneven stator teeth height, therefore flux bidirectional modulating effect can be achieved, which is the basis to realize effective coupling among the magnetic fields excited by the PMs, dc field current, and armature current. Apart from the fundamental component of the magnetic field, a wealth of field harmonics is produced due to the noneven magnetic reluctance distribution. Harmonics with the same PPN and same rotational speed can couple together to produce a steady electromagnetic torque. In order to reveal the working principle of the proposed HE-FBMG, the flux density, flux linkage, back EMF, and electromagnetic torque are investigated analytically.

A. Excitation Flux Density in the Air Gap

The magneticmotive force (MMF) produced by the rotor PMs and field currents are expressed by

$$F_f\left(\theta\right) = \sum_{i=1,3,5}^{\infty} F_{fi} \cos\left(i\frac{Ns}{2}\theta\right) \tag{8}$$

$$F_{\text{PM}}\left(\theta, t\right) = \sum_{j=1,3,5}^{\infty} F_{\text{PM}j} \cos jpr\left(\theta - \Omega rt - \theta 0\right) \tag{9}$$

where i and j are the order of harmonics, Ns refers to the stator slot number, θ,Ωr, and $\theta 0$ are air-gap circumferential position, the rotor speed in radian per second, and the initial rotor teeth position, respectively, $F_{\text{PM}j}$ is the amplitude of the jth MMF harmonic of the rotor PMs, F_{fi} is the amplitude of the ith MMF harmonic produced by the field current and can be expressed as

$$F_{fi} = \frac{4N_{fIf}}{i\pi} \sin\left(ibso\frac{\pi}{2}\right) \tag{10}$$

where N_f is the turns of field winding, I_f is the field current, and bso is the stator slot opening. When calculating the air-gap permeance, the uneven permeance distribution of both the stator and the rotor should be considered. The air-gap permeance function of the stator can be expressed as

$$\Lambda s\left(\theta\right) = \Lambda s0 - \sum_{v=1}^{\infty} \Lambda sv \cos\left(v\frac{Ns}{2}\theta\right) \tag{11}$$

where $\Lambda s0$ and Λsv are the average value and amplitude of the vth stator permeance harmonic, respectively, and the air-gap permeance function of the rotor can be calculated in a similar

way, as given by

$$\Lambda r\left(\theta,t\right)=\Lambda r0-\sum_{n=1}^{\infty}\Lambda rn\cos\left(npr\left(\theta-\Omega rt-\theta0\right)\right) \quad (12)$$

where $\Lambda r0$ and Λrn are the average value and amplitude of the nth rotor permeance harmonic, respectively. The air-gap permeance of the proposed HE-FBMG can be obtained by multiplying (11) and (12), and is expressed as

$$\begin{aligned}\Lambda\left(\theta,t\right)&=\Lambda s\left(\theta\right)\Lambda r\left(\theta,t\right)\\&=\Lambda s0\Lambda r0-\Lambda r0\sum_{v=1}^{\infty}\Lambda sv\cos\left(v\frac{Ns}{2}\theta\right)\\&-\Lambda s0\sum_{n=1}^{\infty}\Lambda rn\cos\left(npr\theta-npr\left(\Omega rt+\theta0\right)\right)\\&+\frac{1}{2}\sum_{v=1}^{\infty}\sum_{n=1}^{\infty}\Lambda sv\Lambda rn\cos\\&\left(\left(npr\pm v\frac{Ns}{2}\right)\theta-npr\left(\Omega rt+\theta0\right)\right). \quad (13)\end{aligned}$$

By multiplying the air-gap permeance given in (13) with the MMF given in (8) and (9), the air-gap flux density excited by the rotor PMs and field currents can be obtained [31], given as

$$\begin{aligned}&B_{\mathrm{PM}}\left(\theta,t\right)=F_{\mathrm{PM}}\left(\theta,t\right)\Lambda\left(\theta,t\right)\\&=\Lambda s0\Lambda r0\sum_{j=1,3,5}^{\infty}\\&F_{\mathrm{PM}j}\cos\left(jpr\theta-jpr\left(\Omega rt+\theta0\right)\right)\\&-\frac{1}{2}\Lambda r0\sum_{j=1,3,5}^{\infty}\sum_{v=1}^{\infty}F_{\mathrm{PM}j}\Lambda sv\cos\\&\left(\left(jpr\pm v\frac{Ns}{2}\right)\theta-jpr\left(\Omega rt+\theta0\right)\right)\\&-\frac{1}{2}\Lambda s0\sum_{j=1,3,5}^{\infty}\sum_{n=1}^{\infty}F_{\mathrm{PM}j}\Lambda rn\cos\\&\left(\left(jpr\pm npr\right)\theta-\left(jpr\pm npr\right)\left(\Omega rt+\theta0\right)\right)\\&+\frac{1}{4}\sum_{j=1,3,5}^{\infty}\sum_{v=1}^{\infty}\sum_{n=1}^{\infty}F_{\mathrm{PM}j}\Lambda sv\Lambda rn\cos\\&\left(\left(jpr\pm npr\pm v\frac{Ns}{2}\right)\theta-\left(jpr\pm npr\right)\left(\Omega rt+\theta0\right)\right)\end{aligned} \quad (14)$$

$$\begin{aligned}&Bf\left(\theta,t\right)=Ff\left(\theta\right)\Lambda\left(\theta,t\right)\\&=\Lambda s0\Lambda r0\sum_{i=1,3,5}^{\infty}F_{fi}\cos\left(i\frac{Ns}{2}\theta\right)\\&-\frac{1}{2}\Lambda r0\sum_{i=1,3,5}^{\infty}\sum_{v=1}^{\infty}F_{fi}\Lambda sv\cos\left(i\frac{Ns}{2}\pm v\frac{Ns}{2}\right)\theta\\&-\frac{1}{2}\Lambda s0\sum_{i=1,3,5}^{\infty}\sum_{n=1}^{\infty}F_{fi}\Lambda rn\\&\cos\left(\left(i\frac{Ns}{2}\pm npr\right)\theta-npr\left(\Omega rt+\theta0\right)\right)\\&+\frac{1}{4}\sum_{i=1,3,5}^{\infty}\sum_{v=1}^{\infty}\sum_{n=1}^{\infty}F_{fi}\Lambda sv\Lambda rn\cos\\&\left(\left(i\frac{Ns}{2}\pm npr\pm v\frac{Ns}{2}\right)\theta-npr\left(\Omega rt+\theta0\right)\right). \quad (15)\end{aligned}$$

One can find that although the field winding is located on the stator, rotating field harmonics can be generated due to the flux modulating effect of the rotor, as shown in the third and fourth items in (15), and it should be noted that the first, third items and the second, fourth items in (14), as well as the first, second items and the third, fourth items in (15) can be combined, and the total excitation flux density in the air-gap equals to the sum of the flux density excited by the rotor PMs and the field current, and can be simplified as

$$\begin{aligned}B\left(\theta,t\right)&=B_{\mathrm{PM}}\left(\theta,t\right)+B_f\left(\theta,t\right)\\&=\sum_{n=1}^{\infty}B_{\mathrm{PM}n}\cos\left(npr\theta-npr\left(\Omega rt+\theta0\right)\right)\\&+\sum_{v=1}^{\infty}B_{fv}\cos\left(v\frac{Ns}{2}\theta\right)\\&+\sum_{n=1}^{\infty}\sum_{v=1}^{\infty}\left(B_{\mathrm{PM}nv}+B_{fnv}\right)\cos\left(\left(npr\pm v\frac{Ns}{2}\right)\theta\right.\\&\left.-npr\left(\Omega rt+\theta0\right)\right)\end{aligned} \quad (16)$$

where $B_{\mathrm{PM}n}$ and $B_{\mathrm{PM}nv}$ are the amplitude of harmonics produced by the rotor PMs, and B_{fn} and B_{fnv} are the amplitude of harmonics produced by the field currents. Both B_{fn} and B_{fnv} are proportional to N_{fIf}, and when field currents are applied, harmonics with $v\frac{Ns}{2}$ pole pairs will be introduced and rotor PM field harmonics with $npr\pm v\frac{Ns}{2}$ pole pairs will be regulated. If no-field current is applied, both B_{fn} and B_{fnv} are zero, the excitation field is only provided by the rotor PMs in this case.

B. Open-Circuit Flux linkage

From Fig. 1(b), one can find that each phase has two coils, which are mechanically located with 180 electric degree difference and have different polarities. Therefore, the open-circuit

flux linkage of each phase can be calculated as (17) shown at the bottom of this page, where rg, ls, and θc are the air-gap radius, stack length, and the initial position of the coil, respectively. One can find that the open-circuit flux linkage contains two items, in which the first item is generated by the rotor PMs only, the second item is generated by the rotor PMs and field currents simultaneously, and can be regulated by controlling the field current

C. Back EMF

The back EMF can be directly obtained by the derivation of the open-circuit flux linkage, given as (18) shown at the bottom of the page.

It can be observed that the back EMF also contains two items, the first item is induced by the rotor PMs only, the second item is induced by the rotor PMs and field currents simultaneously, which can be regulated by controlling the field current.

IV. Control Strategy

In traditional WPGS, the output power of the generator should be rectified by the thyristor-based-controlled rectifier, which is the hardware basis of the control process. In the proposed HE-FBMG-based WPGS, the control process can be achieved by controlling the field current, which is much simpler and thyristor-based-controlled rectifier in traditional WPGS can be replaced with diode-based-uncontrolled rectifier, so the cost of rectifier can be reduced accordingly.

A. Constant Voltage Control

Fig. 2(a) shows the control block of constant voltage control, which is suitable for variable-speed constant voltage applications. The output power of the armature winding is rectified for dc power charging. The dc charging voltage is a feedback and compared with the reference dc charging voltage in the constant voltage controller. According to the error of reference and feedback dc charging voltage, the constant voltage controller generates the reference field current, which then compared with the feedback field current and control the dc power supply. The reference dc charging voltage is the voltage when the generator runs at a certain speed and no-field current is applied, which can be adjusted according to the load requirement. Using this constant voltage control, the dc charging voltage of the proposed HE-FBMG-based WPGS can be maintained at a certain level when the wind speed varies.

B. MPPT Control

As shown in (3), the power coefficient Cp should be as large as possible in order to capture more wind power. According to the research reported in [32], the power coefficient is a nonlinear function of the wind speed and blade shaft speed. Corresponded to each wind speed, there is an optimal shaft speed which has the largest power coefficient. The MPPT control is to make the generator run at the optimal rotating speeds when the wind speed varies, so the wind blade can capture the maximum wind power. In traditional WPGS, the MPPT control is achieved by controlling the controlled rectifier. In the proposed HE-FBMG-based WPGS, the MPPT control can be achieved by controlling the field current. The scheme of MPPT control is given in Fig. 2(b), compared with traditional WPGS using vector control and thyristor-based-controlled rectifier, the

$$\Psi(t) = rgls\int_{\theta c-\frac{bso}{2}}^{\theta c+\frac{bso}{2}} B(\theta,t)\,d\theta - rgls\int_{\pi+\theta c-\frac{bso}{2}}^{\pi+\theta c+\frac{bso}{2}} B(\theta,t)\,d\theta$$

$$= 4rgls\left\{\begin{array}{l}\sum_{n=1}^{\infty}\frac{B_{\mathrm{PM}n}}{npr}\sin\left(npr\frac{bso}{2}\right)\cos\left(npr\theta c - npr\left(\Omega rt+\theta 0\right)\right)\\ +\sum_{n=1}^{\infty}\sum_{v=1}^{\infty}\frac{B_{\mathrm{PM}nv}+B_{fnv}}{npr\pm v\frac{Ns}{2}}\sin\left(\left(npr\pm v\frac{Ns}{2}\right)\frac{bso}{2}\right)\cos\left(\left(npr\pm v\frac{Ns}{2}\right)\theta c - npr\left(\Omega rt+\theta 0\right)\right)\end{array}\right\} \quad (17)$$

$$e(t) = \frac{d\Psi(t)}{dt}$$

$$= 4rgls\left\{\begin{array}{l}\sum_{n=1}^{\infty}B_{\mathrm{PM}n}\Omega r\sin\left(npr\frac{bso}{2}\right)\sin\left(npr\theta_{ph} - npr\left(\Omega rt+\theta 0\right)\right)\\ +\sum_{n=1}^{\infty}\sum_{v=1}^{\infty}\frac{B_{\mathrm{PM}nv}+B_{fnv}}{npr\pm v\frac{Ns}{2}}npr\Omega r\sin\left(\left(npr\pm v\frac{Ns}{2}\right)\frac{bso}{2}\right)\sin\left(\left(npr\pm v\frac{Ns}{2}\right)\theta_{ph} - npr\left(\Omega rt+\theta 0\right)\right)\end{array}\right\} \quad (18)$$

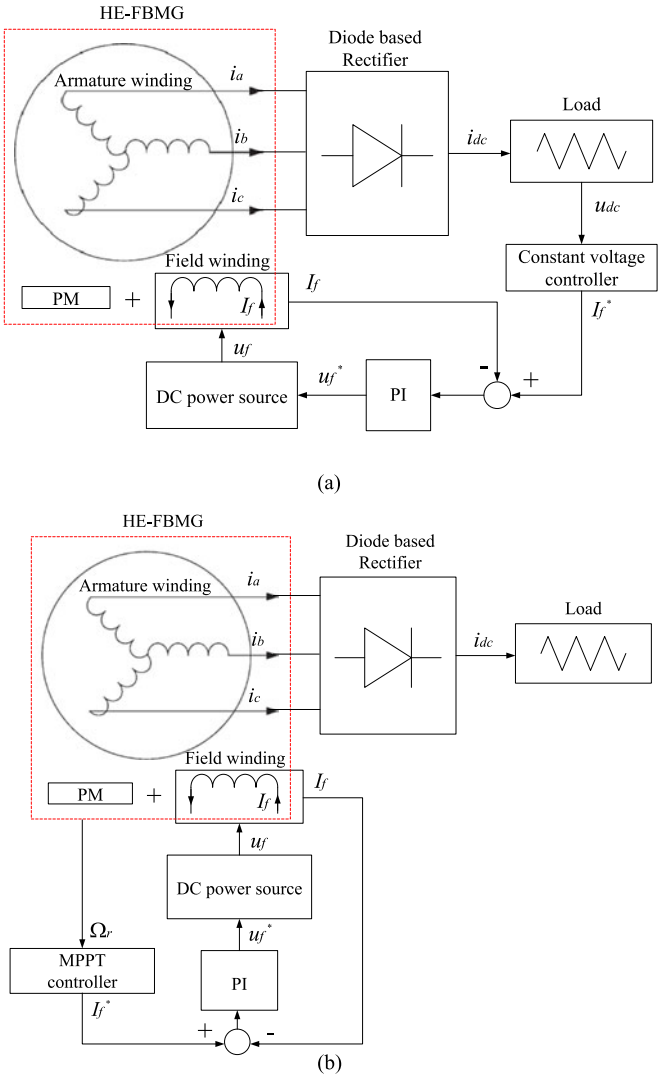

Fig. 2. Control strategies of the proposed HE-FBMG-based WPGS. (a) Constant voltage control. (b) MPPT control.

proposed HE-FBMG-based WPGS has simplified control method and hardware.

V. Finite-Element Analysis

A. Design Optimization

As can be seen from Fig. 1(a), no gearbox is used in the proposed HE-FBMG-based WPGS, the wind blade is directly connected to the rotor shaft of the HE-FBMG, and, therefore, high torque density is a desirable feature for the HE-FBMG. Meanwhile, high efficiency is also desired in order to generate more electric energy, and the torque ripple should be as low as possible so as to reduce the vibration and improve the reliability. To achieve better overall electromagnetic performances, the proposed HE-FBMG is optimal designed using an ITS algorithm, the flowchart of the optimization process is shown in Fig. 3. Three objectives are investigated, which include the

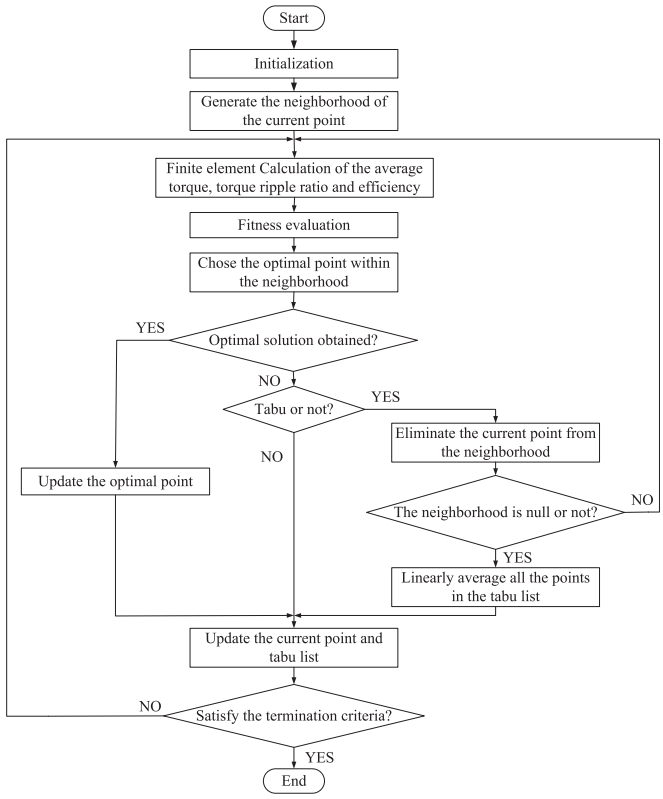

Fig. 3. Flowchart of the optimization process.

output torque $f1$, the efficiency $f2$, and the torque ripple ratio $f3$. The optimal design problem is formulated as

$$\min\left\{-f1\left(x\right),-f2\left(x\right),f3\left(x\right)\right\},\ \ x\in F \tag{19}$$

where x refers to the design parameters, F refers to the range of the design variables. The torque ripple ratio can be expressed in (20), where $T\max$ and $T\min$ are the maximum value and minimum value of the output torque, respectively

$$f3\left(x\right)=\frac{T\max-T\min}{f1\left(x\right)}. \tag{20}$$

The parameterized FE model of the proposed HE-FBMG is built using Maxwell package. During optimization, the overall diameter and stack length are fixed at 90 and 80 mm, respectively. The optimization results of the torque ripple ratio and the average output torque are given in Fig. 4. One can hardly discover identical relationships between the torque ripple ratio and the average torque. Fig. 5 shows the relationship between the efficiency and the average output torque, it can be easily observed that the efficiency is positive correlated with the average output torque. The point with maximum average torque also has the maximum efficiency, and, therefore, the efficiency and the average output torque can be combined into one single objective during optimization.

After the aforementioned multiobjective optimization, the proposed HE-FBMG is optimized through single objective optimization, and the objective is to achieve the largest output

TABLE I
DESIGN PARAMETERS

Parameters	Value
Stator outside diameter (mm)	90
Stator inside diameter (mm)	59.2
Rotor outside diameter (mm)	58.2
Rotor inside diameter (mm)	30
Length of air gap (mm)	0.5
Stack length (mm)	80
Height difference of stator teeth (mm)	2.5
Width of stator teeth (mm)	5.5
Rotor PM ratio	0.5
Thickness of rotor PMs (mm)	4.1
PPN of armature winding	5
PPN of field winding	6
PPN of rotor PMs	11
Number of stator slots	12
Number of phases	3
Remanence of NdFeB (T)	1.2
Relative permeability of NdFeB	1.05

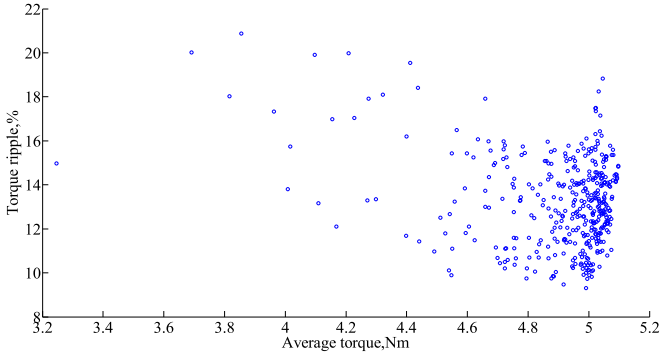

Fig. 4. Relationship between the torque ripple ratio and average torque.

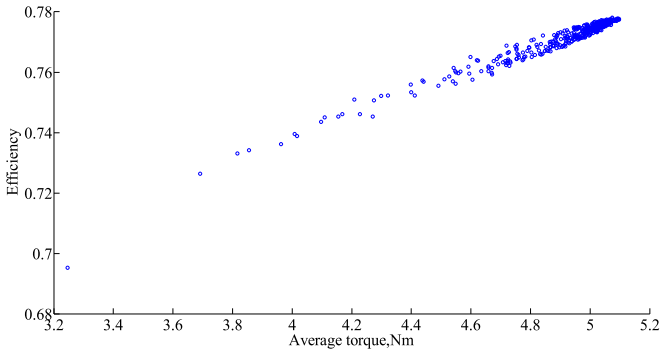

Fig. 5. Relationship between the efficiency and average torque.

torque when the excitation current density is fixed at 8 A/mm^2. The constraint during optimization is that the torque ripple ratio should be lower than 15%. Fig. 6 shows the average output torque and torque ripple ratio at different iterative number. It can be observed that the optimization can converge within 20 iterations and all the torque ripple ratios are lower than 15%, which consists with the constraint and shows the effectiveness of the optimization method. One can find that the proposed machine can achieve good overall performances after optimization.

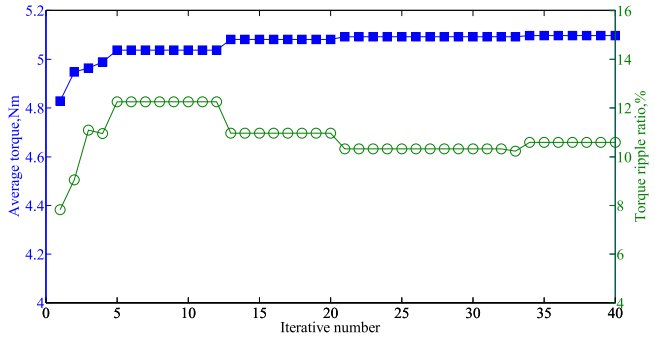

Fig. 6. Average output torque at different iterative number.

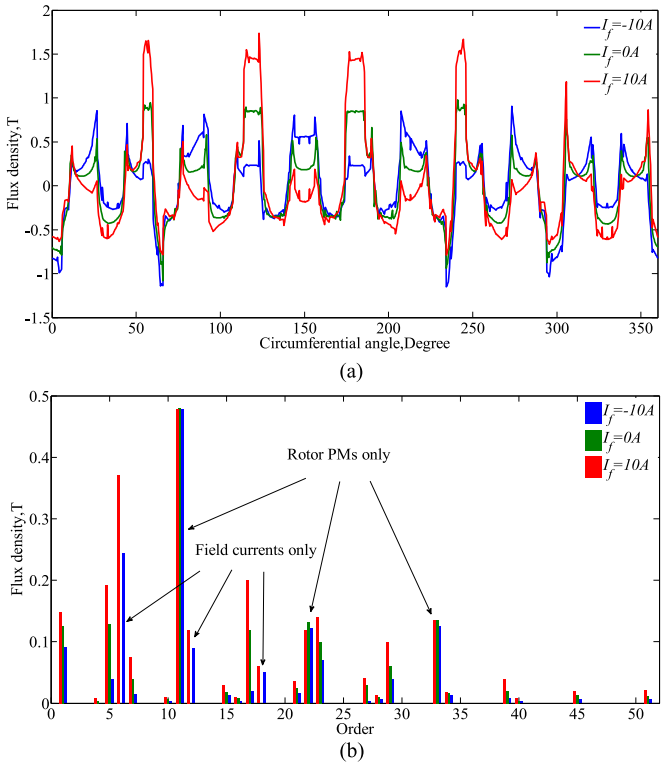

Fig. 7. Open-circuit air-gap flux density distributions and harmonics. (a) Flux density distributions. (b) Harmonics.

The final design parameters can be obtained and output by the optimization algorithm, which are listed in Table I.

B. Performance Analysis

The electromagnetic performances of the proposed HE-FBMG are comprehensively investigated using FEM. First, the excitation field provided by the rotor PMs and field currents is investigated, the air-gap flux density distribution and the harmonic spectrum is given in Fig. 7. One can find that the air-gap flux can be effectively regulated by the field current, both flux strengthening and flux weakening can be achieved by inversing the polarity of the field current. When investigating the harmonic spectrum, only low-order harmonics with $n = 1, 2, 3$ and $v = 1, 2, 3$ are considered. The results show a good agreement with the theoretical derivation given in (16). The harmonics with

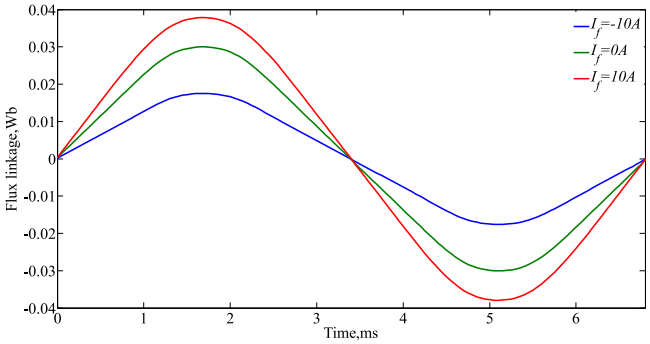

Fig. 8. Open-circuit flux-linkage waveforms.

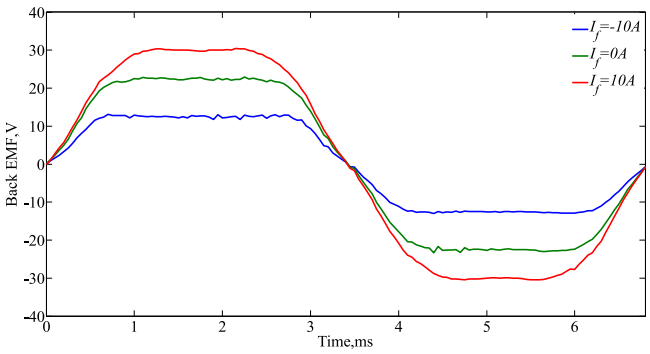

Fig. 9. No-load back-EMF waveforms.

11, 22, and 33 PPN are only generated by the rotor PMs and will not be regulated by the field current. The harmonics with 6, 12, and 18 PPN are only generated by the field current, and the amplitude of these harmonics is zero when no-field current is applied, as shown in the green bar of Fig. 7(b). Other harmonics are generated by both the rotor PMs and the field current, and, therefore, these harmonics can be effectively regulated by controlling the field current.

Fig. 8 shows the open-circuit flux linkage waveforms of with/without field current. One can find that the flux linkage can be effectively regulated through the field current, and by inversing the polarity of the field current, both flux strengthening and flux weakening can be achieved. Similar phenomenon can be observed in the back-EMF waveforms shown in Fig. 9. Therefore, by controlling the field current, the proposed HE-FBMG can achieve constant output voltage when runs at different speeds. Fig. 10 shows the stationary torque waveforms, in which the armature current density is 8 A/mm^2 and the rotor is locked. It can be seen that the output torque can be regulated by the field current as well, when applied with field strengthening current, the output torque of the proposed HE-FBMG can be improved. Fig. 11 shows the torque–current waveforms, no-field current is applied in this case, and the armature current density varies from 2 to 20 A/mm^2. One can find that the output torque of the proposed HE-FBMG is greatly influenced by the current density. When the cooling condition is improved and large current density can be applied, the torque capability of the proposed generator can be increased.

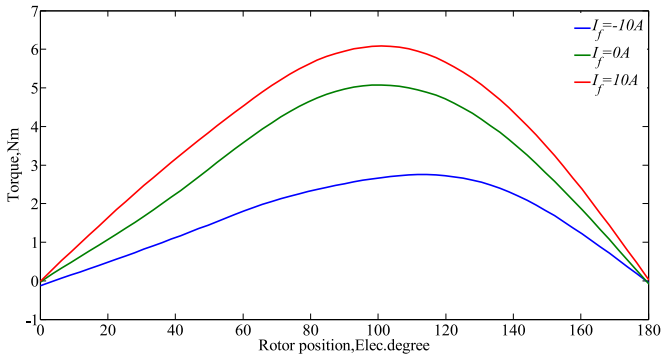

Fig. 10. Stationary torque waveforms.

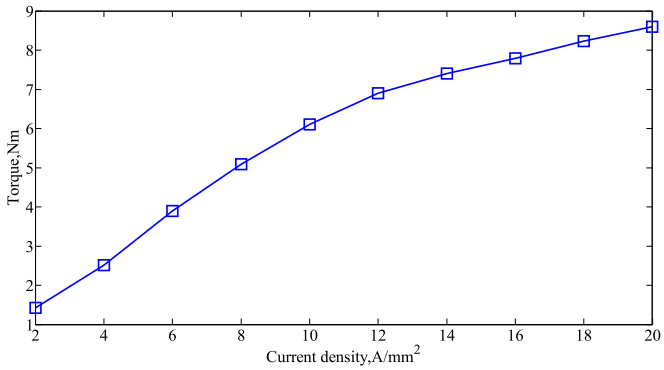

Fig. 11. Torque–current waveforms.

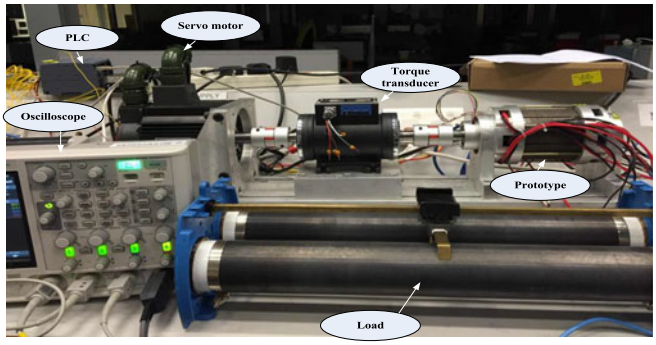

Fig. 12. Test bench of the proposed HE-FBMG-based WPGS.

VI. Experimental Validation

In order to verify the proposed HE-FBMG-based WPGS, a prototype of the HE-FBMG is made and the test bench is shown in Fig. 12. The design parameters of the prototype are exactly the same as the parameters given in Table I. It should be noted that this prototype is only used to validate the proposed design, it cannot be used in a real WPGS because it is a scale-down prototype and its rotor PPN is small. The proposed machine concept can be used in real WPGS when designed with large size and large rotor PPN. The generator is driven by a servo motor, which is controlled by a Siemens 1212C PLC controller stored with the wind turbine parameters and wind curves, and the load is provided by a slide rheostat.

The back-EMF waveforms when the proposed machine running at 800 r/min and applied with different field currents are

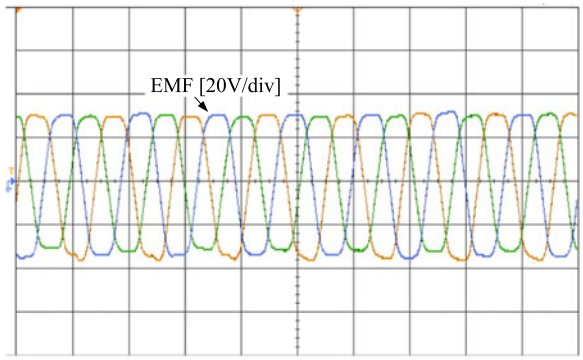

(a)

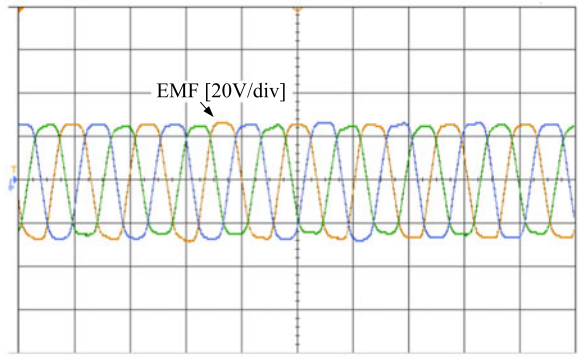

(b)

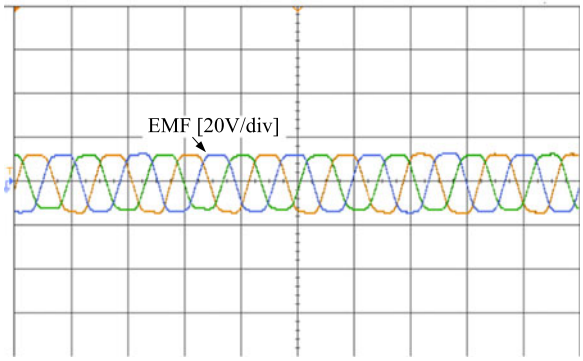

(c)

Fig. 13. Measured EMF waveforms when applied with different field currents. (a) $If = 10$ A. (b) $If = 5$ A. (c) $If = -10$ A.

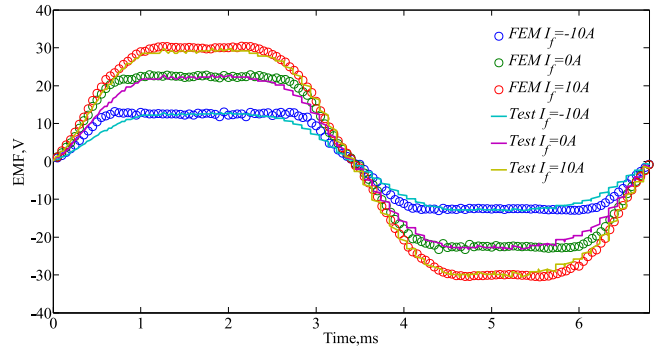

Fig. 14. Comparison of EMF waveforms.

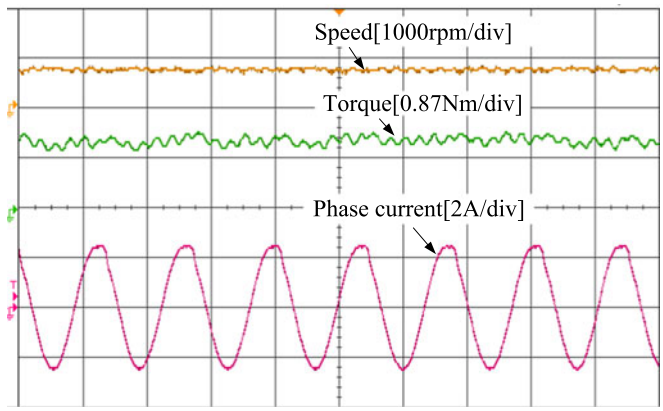

Fig. 15. Generator torque, speed, and phase current when the load resistance is 20 Ω.

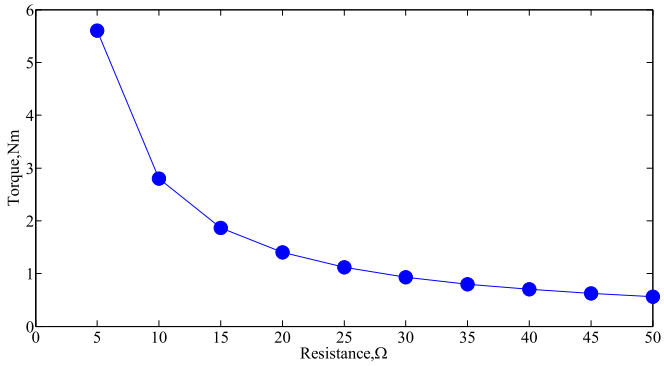

Fig. 16. Generator torque at different load resistances.

tested and given in Fig. 13. It can be observed that the back EMF can be effectively regulated by the field current. The EMF waveforms are not purely sinusoidal and balanced due to the unsymmetrical flux density distribution. There may also exist slight mechanical errors during manufacturing and assembling. Fig. 14 shows the comparison of EMF waveforms when the proposed generator is applied with positive-field current, no-field current, and negative-field current. One can find a good agreement between the test results and the simulation results. The steady-state performances when no-field current is applied are studied. Fig. 15 shows the generator torque and phase current when the generator runs at 800 r/min and the load resistance is 20 Ω. It is shown that the proposed generator can work stably and sinusoidal phase current can be obtained. Keeping the rotating speed unchanged, the generator torque at different load resistances are tested and given in Fig. 16. One can find that with the increasing of load resistance, the generator torque reduces because the increasing of load resistance reduces phase current. Changing the load resistance to 35 Ω, the steady-state generator torque, rotating speed, output dc voltage, and output dc current are all shown on the oscilloscope, as given in Fig. 17. Again, we can find that the proposed HE-FBMG-based WPGS can generate smooth dc voltage and dc current, therefore is very suitable for dc power supply.

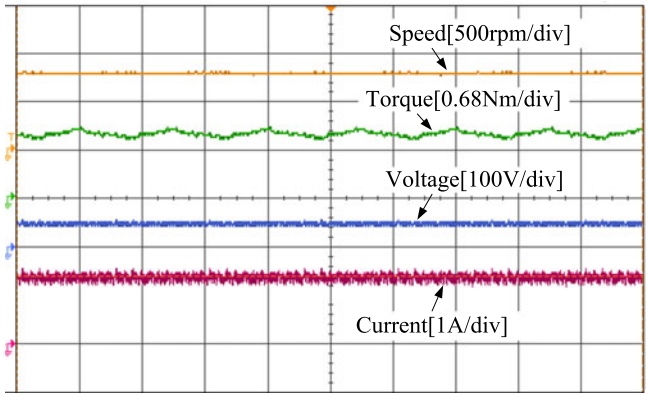

Fig. 17. Generator torque, speed, dc voltage, and dc current when the load resistance is 35 Ω.

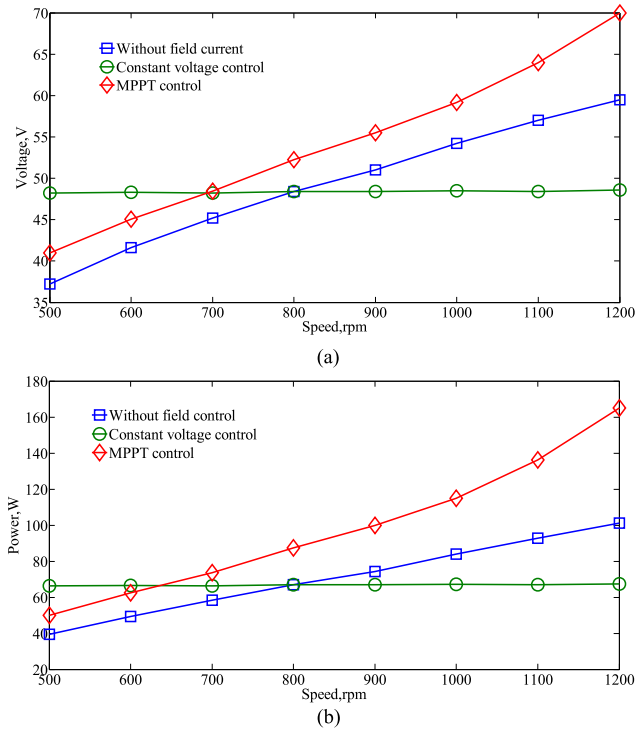

Fig. 18. DC charging voltage and output dc power when the generator speed varies. (a) DC charging voltage. (b) Output dc power.

The dc charging voltage and output dc power are given in Fig. 18, when the proposed generator runs at different speeds and load resistance is 35 Ω. Three operations are investigated, which include field winding open circuited, constant voltage control, and MPPT control. One can find that when no-field current is applied, the dc charging voltage increases almost linearly with the increasing of the rotor speed. When using constant voltage control, the proposed HE-FBMG can maintain the dc charging voltage at a certain level, hence very suitable for variable-speed constant voltage applications. When using MPPT control, the proposed HE-FBMG-based WPGS can get the optimal power point and the output power can be improved effectively. The experimental results well validate the proposed design, and the final performances of the proposed HE-FBMG are given in Table II.

TABLE II
DESIGNED MACHINE RATED VALUES

Items	HE-FBMG
Rated speed (r/min)	800
Rated torque (N·m)	4.7
Rated power (W)	384
Rated voltage (V)	48
Rated current (A)	8

VII. CONCLUSION

In this paper, a novel hybrid-excited generator with flux-bidirectional-modulating effect is proposed for WPGS. With the proposed generator, thyristor-based-controlled rectifier in traditional WPGS can be replaced with diode-based-uncontrolled rectifier, which can reduce the hardware cost. Compared with existing conventional HEMs with both PMs and field coils on the stator, the proposed HE-FBMG can achieve better allocation of PM magnetic loading and electric loading. The spaces used to locate PMs and windings can be increased, which can contribute to high torque density design. The demagnetization risk of PMs is also reduced because the PMs are not directly exposed in the stator thermal field. Bidirectional-flux-modulating effect is incorporated into the proposed design, which guarantees effective magnetic coupling among the magnetic fields excited by the PMs, field coils, and armature windings. Both constant voltage control and MPPT control can be achieved by controlling the field current, the control process is simplified. The analytical model of the proposed generator is established, which can give an insight into the working principle and flux regulating theory. The control strategies are discussed, and an ITS algorithm is used to optimal design the proposed generator. The electromagnetic performances are preliminary investigated using FEM and verified through experiment tests.

REFERENCES

[1] J. K. Kaldellis and D. Zafirakis, "The wind energy evolution: A short review of a long history," *Renew. Energy*, vol. 36, pp. 1887–1901, 2011.
[2] B. R. Karthikeya and R. J. Schütt, "Overview of wind park control strategies," *IEEE Trans. Sustainable Energy*, vol. 5, no. 2, pp. 416–422, Apr. 2014.
[3] M. Liserre, R. Cardenas, M. Molinas, and J. Rodriguez, "Overview of multi-MW wind turbines and wind parks," *IEEE Trans. Ind. Electron.*, vol. 58, no. 4, pp. 1081–1095, Apr. 2011.
[4] H. Polinder, J. A. Ferreira, B. B. Jensen, A. B. Abrahamsen, K. Atallah, and R. A. McMahon, "Trends in wind turbine generator systems," *IEEE J. Emerg. Sel. Topics Power Electron.*, vol. 1, no. 3, pp. 174–185, Sep. 2013.
[5] GWEC. 2016. [Online]. Available: http://www.gwec.net/
[6] Q. Wang and S. Niu, "Overview of flux-controllable machines: Electrically excited machines, hybrid excited machines and memory machines," *Renew. Sustainable Energy Rev.*, vol. 68, pp. 475–491, 2017.
[7] Y. Liu, S. Niu, and W. Fu, "Design of an electrical continuously variable transmission based wind energy conversion system," *IEEE Trans. Ind. Electron.*, vol. 63, no. 11, pp. 6745–6755, Nov. 2016.
[8] X. Luo and S. Niu, "A novel contra-rotating power split transmission system for wind power generation and its dual MPPT control strategy," *IEEE Trans. Power Electron.*, vol. 32, no. 9, pp. 6924–6935, Sep. 2017.
[9] H. Jagau, M. A. Khan, and P. S. Barendse, "Design of a sustainable wind generator system using redundant materials," *IEEE Trans. Ind. Appl.*, vol. 48, no. 6, pp. 1827–1837, Nov./Dec. 2012.

[10] J. Ojeda, M. G. Simoes, G. Li, and M. Gabsi, "Design of a flux-switching electrical generator for wind turbine systems," *IEEE Trans. Ind. Appl.*, vol. 48, no. 6, pp. 1808–1816, Nov./Dec. 2012.
[11] R. Cárdenas, R. Peña, P. Wheeler, J. Clare, and G. Asher, "Control of the reactive power supplied by a WECS based on an induction generator fed by a matrix converter," *IEEE Trans. Ind. Electron.*, vol. 56, no. 2, pp. 429–438, Feb. 2009.
[12] G. Abad, M. A. Rodriguez, G. Iwanski, and J. Poza, "Direct power control of doubly-fed-induction-generator-based wind turbines under unbalanced grid voltage," *IEEE Trans. Power Electron.*, vol. 25, no. 2, pp. 442–452, Feb. 2010.
[13] K. Rothenhagen and F. W. Fuchs, "Doubly fed induction generator model-based sensor fault detection and control loop reconfiguration," *IEEE Trans. Ind. Electron.*, vol. 56, no. 10, pp. 4229–4238, Oct. 2009.
[14] J. Lopez, E. Gubia, P. Sanchis, X. Roboam, and L. Marroyo, "Wind turbines based on doubly fed induction generator under asymmetrical voltage dips," *IEEE Trans. Energy Convers.*, vol. 23, no. 1, pp. 321–330, Mar. 2008.
[15] J. Zhang, Z. Chen, and M. Cheng, "Design and comparison of a novel stator interior permanent magnet generator for direct-drive wind turbines," *IET Renew. Power Gener.*, vol. 1, pp. 203–210, 2007.
[16] H. Polinder, F. F. Van der Pijl, G.-J. De Vilder, and P. J. Tavner, "Comparison of direct-drive and geared generator concepts for wind turbines," *IEEE Trans. Energy Convers.*, vol. 21, no. 3, pp. 725–733, Sep. 2006.
[17] I. A. A. Afinowi, Z. Q. Zhu, Y. Guan, J. C. Mipo, and P. Farah, "Hybrid-excited doubly salient synchronous machine with permanent magnets between adjacent salient stator poles," *IEEE Trans. Magn.*, vol. 51, no. 10, Oct. 2015, Art. no. 8107909.
[18] F. G. Capponi, G. Borocci, G. De Donato, and F. Caricchi, "Flux regulation strategies for hybrid excitation synchronous machines," *IEEE Trans. Ind. Appl.*, vol. 51, no. 5, pp. 3838–3847, Sep./Oct. 2015.
[19] B. Gaussens, E. Hoang, M. Lecrivain, P. Manfe, and M. Gabsi, "A hybrid-excited flux-switching machine for high-speed DC-alternator applications," *IEEE Trans. Ind. Electron.*, vol. 61, no. 6, pp. 2976–2989, Jun. 2014.
[20] C. Zhihui, W. Bo, C. Zhe, and Y. Yangguang, "Comparison of flux regulation ability of the hybrid excitation doubly salient machines," *IEEE Trans. Ind. Electron.*, vol. 61, no. 7, pp. 3155–3166, Jul. 2014.
[21] W. Yu and D. Zhiquan, "Hybrid excitation topologies and control strategies of stator permanent magnet machines for DC power system," *IEEE Trans. Ind. Electron.*, vol. 59, no. 12, pp. 4601–4616, Dec. 2012.
[22] X. Liu, H. Lin, Z. Q. Zhu, C. Yang, S. Fang, and J. Guo, "A novel dual-stator hybrid excited synchronous wind generator," *IEEE Trans. Ind. Appl.*, vol. 45, no. 3, pp. 947–953, May/Jun. 2009.
[23] F. Ying, K. T. Chau, and S. Niu, "Development of a new brushless doubly fed doubly salient machine for wind power generation," *IEEE Trans. Magn.*, vol. 42, no. 10, pp. 3455–3457, Oct. 2006.
[24] Z. Xiaoyong, C. Ming, H. Wei, Z. Jianzhong, and Z. Wenxiang, "Design and analysis of a new hybrid excited doubly salient machine capable of field control," in *Proc. 2006 IEEE 41st IAS Annu. Meet. Conf. Rec. Ind. Appl. Conf.*, 2006, pp. 2382–2389.
[25] Z. Chen and N. Zhou, "Flux regulation ability of a hybrid excitation doubly salient machine," *Electr. Power Appl., IET*, vol. 5, pp. 224–229, 2011.
[26] Q. Wang and S. Niu, "A novel hybrid-excited dual-PM machine with bi-directional flux modulation," IEEE Trans. Energy Convers., vol. 32, no. 2, pp. 424–435, Jun. 2017.
[27] S. L. Ho, Y. Shiyou, N. Guangzheng, and H. C. Wong, "An improved Tabu search for the global optimizations of electromagnetic devices," *IEEE Trans. Magn.*, vol. 37, no. 5, pp. 3570–3574, Sep. 2001.
[28] W. Qingsong, N. Shuangxia, H. Siu Lau, F. Weinong, and Z. Shuguang, "Design and analysis of novel magnetic flux-modulated mnemonic machines," *Electr. Power Appl., IET*, vol. 9, pp. 469–477, 2015.
[29] S. L. Ho, Q. S. Wang, S. X. Niu, and W. N. Fu, "A novel magnetic-geared tubular linear machine with halbach permanent-magnet arrays for tidal energy conversion," *IEEE Trans. Magn.*, vol. 51, no. 11, Nov. 2015, Art. no. 8113604.
[30] K. Atallah and D. Howe, "A novel high-performance magnetic gear," *IEEE Trans. Magn.*, vol. 37, no. 4, pp. 2844–2846, Jul. 2001.
[31] Z. Wu and Z. Zhu, "Analysis of air-gap field modulation and magnetic gearing effects in switched flux permanent magnet machines," *IEEE Trans. Magn.*, vol. 51, no. 5, pp. 1–12, May 2015.
[32] V. Nayanar, N. Kumaresan, and N. A. Gounden, "A single-sensor-based MPPT controller for wind-driven induction generators supplying DC microgrid," *IEEE Trans. Power Electron.*, vol. 31, no. 2, pp. 1161–1172, Feb. 2016.

Qingsong Wang received the B.Sc. degree in vehicle engineering from the College of Automotive Engineering, Jilin University, Changchun, China, in 2012, and the M.Sc. degree in vehicle system dynamics from the School of Automotive Studies, Tongji University, Shanghai, China, in 2015. He is currently working toward the Ph.D. degree in design and control of electrical machines in the Department of Electrical Engineering, The Hong Kong Polytechnic University, Kowloon, Hong Kong.

His research interests include design of novel electric machines, EV/HEV propulsion, and renewable energy systems.

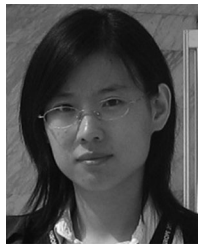

Shuangxia Niu (M'15) received the B.Sc. and M.Sc. degrees in electrical engineering from the School of Electrical Engineering and Automation, Tianjin University, Tianjin, China, in 2002 and 2005, respectively, and the Ph.D. degree in electrical engineering from the Department of Electrical and Electronic Engineering, The University of Hong Kong, Kowloon, Hong Kong, in 2009.

Since 2009, she has been with The Hong Kong Polytechnic University, Kowloon, where she is currently an Assistant Professor in the Department of Electrical Engineering. She has authored or coauthored more than 60 papers in leading journals. Her research interests include design and control of novel electrical machines and drives, renewable energy conversion systems, and applied electromagnetics.